

Recursive Polynomial Method for Fast Collision Avoidance Maneuver Design

ZENO PAVANELLO, LAURA PIROVANO and ROBERTO ARMELLIN

Te Punaha Atea - Space Institute, The University of Auckland, Auckland, New Zealand

Abstract— A simple and reliable algorithm for collision avoidance maneuvers (CAMs), capable of computing impulsive, multi-impulsive, and low-thrust maneuvers, is proposed. The probability of collision (PoC) is approximated by a polynomial of arbitrary order as a function of the control, transforming the CAM design into a polynomial program. The solution procedure is initiated by computing the CAM via a first-order greedy optimization approach, wherein the control action is applied in the direction of the gradient of PoC to maximize its change. Successively, the polynomial is truncated at higher orders, and the solution of the previous order is used to linearize the constraint. This enables achieving accurate solutions even for highly nonlinear safety metrics and dynamics. Since the optimization process comprises only polynomial evaluations, the method is computationally efficient, with run times typically below 1 s. Moreover, no restrictions on the considered dynamics are necessary; therefore, results are shown for Keplerian, J2, and circular restricted three-body problem dynamics.

Index Terms— Fuel optimal control, Nonlinear Programming, Optimization Methods, Polynomial Approximation, Space Vehicle Control

I. INTRODUCTION

According to the most recent European Space Agency (ESA) Space Debris report [1], the number of cataloged resident space objects is over 32,000. This exponential increase, fueled by spacecraft miniaturization and the

Manuscript received May 16, 2024; revised XXXXX 00, 0000; accepted XXXXX 00, 0000.

© 2024 IEEE. Personal use of this material is permitted. Permission from IEEE must be obtained for all other uses, in any current or future media, including reprinting/republishing this material for advertising or promotional purposes, creating new collective works, for resale or redistribution to servers or lists, or reuse of any copyrighted component of this work in other works.

This work has been submitted to the IEEE for possible publication. Copyright may be transferred without notice, after which this version may no longer be accessible.

The codes related to this work can be downloaded for reproducibility at <https://github.com/zenop95/Recursive-polynomial-CAM-design/releases/tag/v1.1.0>.

(Corresponding author: Z. Pavanello).

deployment of mega-constellations like Starlink, is reshaping how we think about space traffic management. A cluttered environment amplifies the frequency of conjunctions and drives the necessity for a commensurate increase in the number of collision avoidance maneuvers (CAMs).

Presently, conjunction analysis and collision avoidance operations are predominantly executed by operators on the ground, leveraging tools and processes refined over the past two decades. While these tools facilitate operational activities, the reliance on human intervention in decision-making processes and maneuvers design will become unsustainable. Therefore, the demand for automated conjunction screening, collision avoidance (CA) decision-making, and CAM design and execution intensifies. This calls for CAM algorithms suitable for autonomous and, potentially, onboard computations providing fuel-optimal maneuvers in a short execution time. This paper aims to address this pressing need by proposing a method for CAM optimization suitable for autonomous applications.

A CAM is performed when operators receive a Conjunction Data Message (CDM) indicating the time of closest approach (TCA) between the satellite and a secondary object and the relevant information of the conjunction. Generally, the estimated probability of collision (PoC) at TCA exceeds a threshold value, and the objective of the CAM is to lower it while minimizing the total Δv . Alternatively, if considerations on the uncertainty of the state of the two objects are not of interest, the conjunction is mitigated by increasing the miss distance at TCA. Previous research has explored various methodologies for optimizing CAMs, often simplifying the problem by assuming small maneuvers [2]. Alfano [3] introduced a CAM analysis tool capable of conducting parametric studies on single-axis and dual-axis maneuvers, while the German Aerospace Center and ESA have developed their own CAM optimization tools with differing degrees of flexibility and optimality [4, 5]. Moreover, recent advancements have seen the emergence of multi-objective approaches for CAM design, enabling comprehensive analyses and the identification of Pareto optimal solutions [6]. Even though very useful for robust and optimal maneuvers computations, all of these solutions are not feasible for autonomous applications because of their high computational load. In recent years, a substantial corpus of research has emerged to devise efficient CAM algorithms. Bombardelli [7] and Bombardelli and Hernando-Ayuso [8, 9] devised analytical and semi-analytical methods to minimize miss distance or collision probability using a single impulse for a given magnitude of Δv , demonstrating promising convergence properties. De Vittori *et al.* proposed an analytical approach for the energy-optimal problem and a semi-analytical one for the fuel-optimal to handle low-thrust CAMs [10], which are particularly relevant given the increasing popularity of electric thrusters [11]. Direct optimization methods have also been extensively utilized to compute CAMs. Misra and Dutta [12] linearize the PoC constraint and

achieve fast but conservative solutions, so they do not guarantee the minimum fuel expenditure. Armellin [13] convexifies the fuel-optimal CAM optimization nonlinear program (NLP) using differential algebra (DA), lossless convexification, and transforming the PoC constraint into a keep-out-zone constraint; the convex program is then solved iteratively, and the original fuel-optimal solution is achieved. Armellin’s method was later extended to solving long-term encounters [14], multiple consecutive encounters [15], and encounters during low-thrust arcs [16].

In this work, we propose an alternative method to design the CAM, which can retain computational speed comparable to semianalytical indirect methods while encompassing flexibility similar to direct methods. We frame the CAM design problem as a polynomial program (PP) by utilizing the energy-optimal objective function and approximating PoC as a high-order Taylor polynomial in the control. This can be represented as a series of impulses or accelerations applied at specified nodes or segments. The PP is solved by leveraging the assumption that high-order terms get smaller in a convergent Taylor series. Thus, starting from a greedy solution of the problem with a linearized PoC constraint, we establish a simple and computationally efficient recursive approach that can achieve quasi-optimal results while accurately meeting the safety constraint. The PP is solved using a succession of solutions of increasing polynomial order. The tensor notation, notably used in astrodynamics problems in recent years to define state transition tensors [17], is adopted to frame the recursive method. DA is used to compute the tensors efficiently. This methodology allows for considering any dynamics, including high-accuracy Earth orbit models and circular restricted three-body problem (CR3BP) models for the Cislunar environment. Given its efficiency, flexibility, and simplicity, this tool could become an important asset for operators to transition towards autonomous CAMs design.

The solution obtained with the proposed recursive method is compared with the interior-point method implemented in MATLAB’s `fmincon` for the fuel-optimal NLP. In this way, the recursive method is proven to be faster than a state-of-the-art solver with limited loss in terms of optimality.

The paper is organized as follows. In Section II, the dynamics models considered for the CAM applications are introduced. Section III sets the NLP using automatic Taylor expansions. The main innovation proposed by this work, i.e., the recursive algorithm to solve the CAM PP, is shown in Section IV. In Section V, operational results are presented, and the comparison with the interior-point solver is discussed. Lastly, in Section VI, conclusions are drawn. The open-source software developed for this work can be consulted and downloaded using the link on the first page.

II. DYNAMICS FRAMEWORKS

This section introduces the framework of the CAM optimization problem dynamics. Different models are considered, depending on the domain in which the CAM needs to be performed and on the degree of accuracy of the modeled environment.

A. Conjunction in the B-plane

This work assumes that the relative velocity between the two satellites at TCA is high. Therefore, the encounter can be regarded as an instantaneous event [13]. A CDM gives the state and covariance matrix of the two satellites involved in the conjunction at TCA. By international standards, a CDM assumes that the states of the two bodies are Gaussian multivariate random variables, so the mean state and covariance are sufficient to describe them. Typically, for Earth orbit conjunctions, the states are expressed in an Earth Centered Inertial (ECI) reference frame; in the Cislunar environment, they are expressed in the synodic reference frame. Therefore, the mean state of the primary is $\mathbf{x}(t_{CA}) = [\mathbf{r}(t_{CA}); \mathbf{v}(t_{CA})]$, while the debris has mean state $\mathbf{x}_s(t_{CA}) = [\mathbf{r}_s(t_{CA}); \mathbf{v}_s(t_{CA})]$. Here, $\mathbf{r}(t_{CA})$, $\mathbf{r}_s(t_{CA})$, $\mathbf{v}(t_{CA})$ and $\mathbf{v}_s(t_{CA}) \in \mathbb{R}^3$ denote the position and velocity of the centers of mass of the objects. Analogously, the covariances of the two objects are \mathbf{C} and $\mathbf{C}_s \in \mathbb{R}^{6 \times 6}$. The relative state is defined as the subtraction of the two absolute states. Since the relative state is of interest only at TCA, we omit the argument

$$\mathbf{x}_{rel} = \mathbf{x}(t_{CA}) - \mathbf{x}_s(t_{CA}), \quad \mathbf{C}_{rel} = \mathbf{C} + \mathbf{C}_s. \quad (1)$$

Note that $\mathbf{x}_{rel} = [\mathbf{r}_{rel}; \mathbf{v}_{rel}]$ and $\mathbf{C}_{rel} = [\mathbf{C}_{rr} \ \mathbf{C}_{rv}; \mathbf{C}_{rv} \ \mathbf{C}_{vv}]$. For the scope of this study, we are only interested in the positional part of the covariance matrix, which will be referred to as $\mathbf{P} = \mathbf{C}_{rr}$ in the following.

Given the short-term nature of the encounter, it can be studied in the B-plane reference frame denoted as \mathcal{B} . \mathcal{B} is centered on the secondary object; the η axis aligns with the direction of the relative velocity of the primary with respect to the secondary, while the $\xi\zeta$ plane is perpendicular to the relative velocity axis. Since the TCA is the moment when the miss distance is minimum, $\mathbf{r}_{rel} \cdot \mathbf{v}_{rel} = 0$ by assumption, indicating that the relative position lies within the $\xi\zeta$ plane. Therefore, for the computation of PoC, we will employ the projection of the relative state and its covariance on the $\xi\zeta$ plane: $\mathbf{r}_{\mathcal{B}} \in \mathbb{R}^2$ and $\mathbf{P}_{\mathcal{B}} \in \mathbb{R}^{2 \times 2}$. The subsequent discussion assumes that all uncertainty is concentrated around the secondary object, while all mass is concentrated around the primary [18].

A conservative way to compute PoC of the encounter is enveloping each of the bodies in a sphere with a radius equal to the largest dimension. The sum of the radii of the two spheres is the hard body radius (HBR), which defines the combined hard body sphere centered in the primary. The projection of this sphere onto the B-plane is the combined hard body circle \mathcal{C}_{HBR} . To compute PoC,

denoted as $P_C \in \mathbb{R}_+$, the probability density function of the projection of the relative position onto the B-plane is integrated over the combined hard-body circle, as follows

$$P_C = \frac{1}{(2\pi)^{3/2} \sqrt{\det(\mathbf{P}_B)}} \cdot \iint_{\mathcal{C}_{\text{HBR}}} \exp\left(-\frac{\mathbf{r}_B^T \mathbf{P}_B^{-1} \mathbf{r}_B}{2}\right) dA. \quad (2)$$

Multiple approaches have been proposed to approximate the integral in Eq. (2) [18]. The results presented in Section V are obtained using Chan's method [19], which approximates PoC through a convergent series that involves equivalent cross-sections. Nonetheless, other methods are present in the literature, and we highlight the fact that our optimization method is agnostic to the PoC model used since the automatic Taylor expansion can deal with any function. Therefore, the following discussion is made without assuming any particular PoC model: in general, for a given HBR, PoC is expressed as a function of the relative position, and the combined covariance in the B-plane at TCA

$$P_C = P_C(\mathbf{r}_B, \mathbf{P}_B). \quad (3)$$

B. Earth Orbit Dynamics

To compute the optimal CAM, starting from the states given by the CDM, the maneuverable satellite is back-propagated up to a suitable time to start executing the maneuver. The algorithm is agnostic to the dynamics model utilized, so any representations of the orbital environment can be employed. Since the time frame is relatively short for typical CAM scenarios, orbital perturbations like high-order gravitational harmonics, atmospheric drag, solar radiation pressure, and third-body attraction do not play a significant role. To showcase the capability of the algorithm, we include the perturbation from the J2 term of the gravitational potential of the planet

$$\begin{aligned} \dot{\mathbf{r}} &= \mathbf{v} \\ \ddot{x} &= -\frac{\mu}{r^3} x (1 + k_{J_2} (1 - 5z^2/r^2)) + u_x, \\ \ddot{y} &= -\frac{\mu}{r^3} y (1 + k_{J_2} (1 - 5z^2/r^2)) + u_y, \\ \ddot{z} &= -\frac{\mu}{r^3} z (1 + k_{J_2} (3 - 5z^2/r^2)) + u_z, \end{aligned} \quad (4)$$

where $\mathbf{r} = [x \ y \ z]^T$, $\mu \in \mathbb{R}_+$ is the gravitational constant of the Earth, $k_{J_2} = \frac{3}{2} \left(\frac{R_E}{r}\right)^2 J_2 \in \mathbb{R}_+$, $R_E \in \mathbb{R}_+$ is the Earth's equatorial radius, $J_2 \in \mathbb{R}_+$ is the Earth's oblateness coefficient, $t \in \mathbb{R}_{[t_0, t_{CA}]}$ is the time domain that goes from an arbitrary starting time t_0 to TCA, and $\mathbf{u} = [u_x \ u_y \ u_z]^T \in \mathbb{R}^3$ is the acceleration control action. The mass loss due to the maneuver is considered negligible because a CAM usually involves a small Δv [8].

C. Cislunar Dynamics

In the cislunar domain, the motion is described by the CR3BP dynamics. The most convenient reference frame

to represent the motion of the satellite is the synodic, which rotates with the same angular speed as the orbital motion of the two main bodies, i.e., the Earth and the Moon. The origin of the synodic reference frame is in the barycenter of the Earth-Moon system; the x axis extends from the origin to the Moon's center of mass, the z axis is in the direction of the angular momentum of the system, and the y axis completes the right-handed triad. In this reference frame, the two main bodies are stationary, and the third body typically moves following a chaotic behavior unless it is in a stable orbit.

The physics of the system is nondimensionalized using the characteristic mass $M = 6.04564 \times 10^{15}$ kg, the characteristic length $D = 384405$ km, and the characteristic time $T = 375677$ s. The equations of motion can be written in compact form in the synodic frame as

$$\begin{aligned} \dot{\mathbf{r}} &= \mathbf{v} \\ \ddot{x} &= 2\dot{y} - \Omega_x + u_x, \\ \ddot{y} &= -2\dot{x} - \Omega_y + u_y, \\ \ddot{z} &= -z - \Omega_z + u_z, \end{aligned} \quad (5)$$

where Ω_x , Ω_y , and Ω_z are the partial derivatives of the effective potential [20].

III. CAM OPTIMIZATION PROBLEM

In this section, the CAM Optimization Problem is set first as an optimal control problem (OCP) and afterward as a NLP.

A. Optimal Control Problem

The fuel-optimal CAM OCP has the objective of finding the minimum control action that can grant a reduction of PoC below an arbitrary threshold. The thrusting opportunities are fixed at predefined times before TCA. These are collected into the set $\mathbb{T} = \{t_0, t_1, \dots, t_N\}$, $N \in \mathbb{N}$. The algorithm proposed in this work is intended to compute maneuvers either using a low-thrust dynamics model or impulsive approximation. In the former case, the optimization variable is the continuous $\mathbf{u}(t)$. In the latter, $\mathbf{u}(t) = \mathbf{0}_3$ at every time, and the control is given by the discrete impulses Δv_i for $i \in \{0, \dots, N\}$. In Fig. 1, the equivalent impulsive and low-thrust schemes are shown: the blue nodes depict the times where the control variables are placed, while the black ones indicate ballistic propagation points. To include both possibilities, in the following, the control variable is denominated

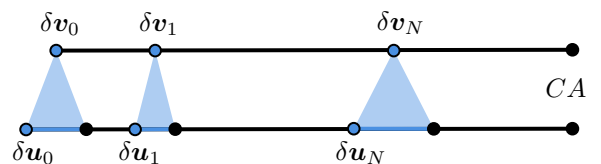


Fig. 1. Impulsive and low-thrust designs.

$\phi \in \mathbb{R}^3$ and its magnitude $\phi \in \mathbb{R}$.

$$\min_{\mathbf{u}(t) \vee \Delta \mathbf{v}_i} J = \begin{cases} \int_{t_0}^{t_N} \|\mathbf{u}(\tau)\| d\tau \\ \sum_{i=0}^{i=N} \|\Delta \mathbf{v}_i\| \end{cases} \quad (6a)$$

$$\text{s.t. Eq. (4) or Eq. (5)} \quad (6b)$$

$$P_C(t) \leq \bar{P}_C \quad (6c)$$

$$\mathbf{r}(t_0) = \mathbf{r}_0 \quad (6d)$$

Eq. (6a) imposes the minimization of the fuel-optimal objective function $J \in \mathbb{R}_+$: the first case is used for low-thrust dynamics, the second one for the multi-impulsive; Eq. (6b) is the dynamics constraint, which depends on the selected model; Eq. (6c) is the PoC constraint, which imposes that PoC must be below the required threshold \bar{P}_C at any time; Eq. (6d) defines the initial position of the satellite, which cannot be altered.

B. Nonlinear Program

Problem (6) is discretized by using a Runge-Kutta 7-8 integration scheme. The initial state \mathbf{x}_0 is yielded by back-propagating the ballistic motion of the primary starting from TCA. The nominal state at subsequent thrusting opportunities can be obtained via successive forward propagations. Therefore, the discretized dynamics equations at any discretization node t_i are generally written

$$\mathbf{x}_i = \mathbf{f}_i(\mathbf{x}_{i-1}, \mathbf{u}_{i-1}, \mathbf{p}) \quad i \in \{1, \dots, N\}, \quad (7)$$

where $\mathbf{f}_i(\cdot) : \mathbb{R}^6 \times \mathbb{R}^3 \times \mathbb{R}^{m_p} \rightarrow \mathbb{R}^6$ is the discretized dynamics function and $\mathbf{p} \in \mathbb{R}^{m_p}$ is a vector of parameters. The discretization assumes a first-order hold for the input action; therefore, the control between two consecutive firing opportunities is constant.

By means of DA, we introduce perturbations on the control variable at each thrusting opportunity ($\phi_i + \delta\phi_i$) in a forward-propagation scheme. Considering a ballistic reference trajectory (no initial control), in the multi-impulsive case, the velocity perturbation is added to the state at every node

$$\mathbf{x}_i = \mathcal{T}^n|_{\mathbf{x}_i}(\mathbf{x}_{i-1}) + [\mathbf{0}_3 \ \delta \mathbf{v}_i]^T \quad i \in \{1, \dots, N\} \quad (8a)$$

$$\mathbf{x}_{p,0} = \mathbf{x}_{p,0} + [\mathbf{0}_3 \ \delta \mathbf{v}_0]^T, \quad (8b)$$

where $\mathcal{T}^n|_{\mathbf{x}_i}(\cdot) : \mathbb{R}^6 \rightarrow \mathbb{R}^6$ is the n^{th} -order Taylor series approximation of \mathbf{x}_i . In the low-thrust case, the acceleration is defined at every node using DA perturbations, and it directly contributes to the dynamics¹

$$\mathbf{x}_i = \mathcal{T}^n|_{\mathbf{x}_i}(\mathbf{x}_{i-1}, \mathbf{u}_{i-1}) \quad i \in \{1, \dots, N\}, \quad (9)$$

where $\mathcal{T}^n|_{\mathbf{x}_i}(\cdot) : \mathbb{R}^6 \times \mathbb{R}^3 \rightarrow \mathbb{R}^6$. A detailed explanation of the use of DA can be found in [21]. As this is a polynomial expansion, its accuracy is inversely proportional

¹As illustrated in Fig. 1, the last node of each low-thrust arc is idle to set where the arc stops. This implies that a low-thrust design is more computationally demanding than an impulsive one since at least two nodes are needed to define the low-thrust arc, while only one is necessary for the impulse.

to the entity of the perturbation and directly proportional to the polynomial order.

Given the dependence of PoC on the relative position at TCA, and the dependence of this from the control history, it is possible to construct a multivariate polynomial representation of PoC as dependent on the control perturbations stacked vector, defined as $\delta\Phi = [\delta\phi_0^T \dots \delta\phi_N^T]^T \in \mathbb{R}^M$, where $M = 3(N+1)$

$$P_C = \mathcal{T}^n|_{P_C}(\delta\Phi), \quad (10)$$

where $\mathcal{T}^n|_{P_C}(\cdot) : \mathbb{R}^M \rightarrow \mathbb{R}$. We define the vector of the control history as

$$\Phi = [\phi_0^T \dots \phi_N^T]^T \in \mathbb{R}^M. \quad (11)$$

A NLP is constructed in the following form

$$\min_{\Phi} \sum_{i=0}^{i=N} \|\phi_i\| \quad (12a)$$

$$\text{s.t. } \mathcal{T}^n|_{P_C}(\Phi) = \bar{P}_C, \quad (12b)$$

where Eq. (12a) is the fuel-optimal objective function and Eq. (12b) is the scalar polynomial PoC constraint. The inequality constraint Eq. (6c) is turned into an equality sign because it is hypothesized that the PoC reduction is proportional to the entity of the maneuver. Problem (12) can be solved using a global optimization tool² or MATLAB's fmincon³.

IV. SEQUENTIAL POLYNOMIAL RECURSIVE METHOD

The recursive method that is proposed in this section is used to solve the energy-optimal counterpart of Problem (12). Therefore, the NLP is converted into a PP by changing the objective function, which becomes quadratic

$$\min_{\Phi} \Phi^T \Phi \quad (13a)$$

$$\text{s.t. } \mathcal{T}^n|_{P_C}(\Phi) = \bar{P}_C. \quad (13b)$$

We employ a recursive approach to find solutions to the PP of increasing polynomial orders. The polynomial is first truncated in the 1st order to obtain an approximate solution; this solution is used as a first guess to solve the problem with a polynomial constraint truncated in the 2nd order. An iterative process is applied to find the second-order solution; when convergence is reached, the recovered solution is fed to a 3rd-order truncated polynomial, and this process is repeated up to the n^{th} order.

A. Mathematical Background

The formulation of the recursive method is based on the use of tensor notation for Taylor expansions. Given a function $g(\cdot) : \mathbb{R}^m \rightarrow \mathbb{R}$, its Taylor expansion can

²<https://yalmip.github.io/tutorial/globaloptimization/>

³<https://au.mathworks.com/help/optim/ug/fmincon.html>

be computed up to an arbitrary order n . The polynomial approximating $g(\cdot)$, as computed on the expansion point $\mathbf{y}^* \in \mathbb{R}^m$ can be written as

$$\mathcal{T}^n \Big|_{g(\mathbf{y})} (\mathbf{y}) = g(\mathbf{y}^*) + \sum_{k=1}^n \frac{1}{k!} \frac{\partial^k g}{\partial \mathbf{y}^k} (\mathbf{y}^*) (\mathbf{y} - \mathbf{y}^*)^k. \quad (14)$$

Eq. (14) is equivalent to writing the polynomial using tensors of increasing orders [22]. The gradient of $g(\cdot)$ is a 1st-order tensor, i.e., a vector; its Hessian is a 2nd-order tensor, i.e., a matrix, and so on. Therefore, it is possible to define the k^{th} -order tensor using k different indices: the vector $\mathbf{a} \in \mathbb{R}^m$ is indexed as a_i ($i \in \{1, \dots, m\}$), the matrix $\mathbf{A} \in \mathbb{R}^{m^2}$ is indexed as $A_{i_1 i_2}$ ($i_1, i_2 \in \{1, \dots, m\}$), the third order tensor $\mathcal{A} \in \mathbb{R}^{m^3}$ is indexed $\mathcal{A}_{i_1 i_2 i_3}$ ($i_1, i_2, i_3 \in \{1, \dots, m\}$), and so on. With this tool, we can now express the k^{th} -order derivatives of $g(\cdot)$ using k^{th} -order tensors. Moreover, since the derivative operation is commutative, these tensors have the useful property of super-symmetry, i.e., they are invariant to permutations of the indices. In the following, the order of the tensor will be indicated as a bracketed superscript, $\mathcal{A}^{(k)}$. Given a tensor $\mathcal{A}^{(k)}$ and a vector $\mathbf{v} \in \mathbb{R}^m$, their multi-linear form $\mathcal{A}^{(k)} \mathbf{v}^k \in \mathbb{R}$ is defined as:

$$\mathcal{A}^{(k)} \mathbf{v}^k = \sum_{i_1, i_2, \dots, i_k=1}^m \mathcal{A}_{i_1 i_2 \dots i_k} v_{i_1} v_{i_2} \dots v_{i_k}, \quad (15)$$

where the notation \mathbf{v}^k refers to the repetition of \mathbf{v} for k times. The summation is only performed over indices that are unique to the right-hand side of the equation. With this knowledge, we can now re-write Eq. (14) using multi-linear forms

$$\mathcal{T}^n \Big|_{g(\mathbf{y})} (\mathbf{y}) = g(\mathbf{y}^*) + \sum_{k=1}^n \mathcal{G}^{(k)} (\mathbf{y} - \mathbf{y}^*)^k, \quad (16)$$

where $\mathcal{G}^{(k)}$ is the k^{th} -order tensor that collects the k^{th} -order derivatives with respect to \mathbf{y} .

If the multiplication by the first tensor mode is eliminated, we obtain a row-vector output⁴, indicated as $\mathcal{A}^{(k)} \mathbf{v}^{k-1} \in \mathbb{R}^m$. Its definition is as follows

$$(\mathcal{A}^{(k)} \mathbf{v}^{k-1})_j = \sum_{i_2, \dots, i_k=1}^m \mathcal{A}_{j i_2 i_3 \dots i_k} v_{i_2} v_{i_3} \dots v_{i_k}, \quad (17)$$

which is valid for each element of the row $j \in \{1, \dots, m\}$.

B. Method

Let us re-write the polynomial $\mathcal{T}^n \Big|_{P_C} (\Phi)$ from Eq. (13b) using the multi-linear forms introduced in Section A

$$\mathcal{T}^n \Big|_{P_C} (\Phi) = P_C^0 + \sum_{k=1}^n \mathcal{F}^{(k)} \Phi^k, \quad (18a)$$

$$\mathcal{F}^{(k)} = \frac{1}{k!} \frac{\partial^k P_C}{\partial \Phi^k} \quad (18b)$$

⁴In the literature it is often assumed to be a column-vector, but a row-vector is preferred for the purpose of this work since it will be used to define a pseudo-gradient.

$$P_C^0 = \mathcal{T}^0 \Big|_{P_C} (\Phi) \quad (18c)$$

where $P_C^0 \in \mathbb{R}$ is PoC of the unperturbed trajectory, i.e., the 0th-order of the Taylor polynomial; $\mathcal{F}^{(k)} \in \mathbb{R}^{M^k}$ - for $k \in \{1, \dots, n\}$ - are symmetric k^{th} -order tensors that represent the contributions of all the k^{th} -order partial derivatives of PoC with respect to Φ . The number of dimensions of the tensor $\mathcal{F}^{(k)}$ is equal to the order of the associated polynomial term, e.g., $\mathcal{F}^{(2)} \in \mathbb{R}^{M^2}$, $\mathcal{F}^{(3)} \in \mathbb{R}^{M^3}$, and so on.

The first-order truncation of Eq. (18a) reads

$$\mathcal{T}^1 \Big|_{P_C} (\Phi) = P_C^0 + (\nabla P_C) \Phi, \quad (19)$$

where $\nabla P_C = \mathcal{F}^{(1)} \in \mathbb{R}^M$ is the gradient of PoC with respect to the stacked control (row vector). The probability gap that needs to be filled by the maneuver is called $\rho \in \mathbb{R}$

$$\rho := \bar{P}_C - P_C^0. \quad (20)$$

Then, the first-order truncation of the equality constraint Eq. (13b) becomes

$$\rho = (\nabla P_C) \Phi. \quad (21)$$

This equation suggests that, in a first-order approximation, a thrust in the direction of the gradient grants the highest possible change in PoC. Therefore, we compute the greedy solution of the first-order constraint as

$$[\Phi]_1 = \frac{\rho}{\nabla P_C} \hat{\nabla} P_C, \quad (22)$$

where ∇P_C is the norm of the gradient, $\hat{\nabla} P_C$ is its direction, and the index 1 indicates that this is a solution to the first-order constraint.

Now, let us assume that a greedy solution has been found for the $(j-1)^{\text{th}}$ -order polynomial program; the generalized process for finding the j^{th} -order solution is as follows. The j^{th} -order truncation of Eq. (13b) is written using the multi-linear form notation from Eq. (18a) and the definition in Eq. (20)

$$\rho = \sum_{k=1}^j \mathcal{F}^{(k)} \Phi^k. \quad (23)$$

In this case, finding a greedy solution is not as simple as in the first-order case because we have a higher-order dependence from Φ . Therefore, successive linearizations of Eq. (23) are carried on until convergence. The iteration number is indicated with $b \in \mathbb{N}$. In the first iteration, the linearization point is the output of the previous order $\tilde{\Phi} = [\Phi]_{j-1}^{\text{end}}$. To express the linearized polynomial, we make use of the multi-linear mode with the exclusion of the first tensor mode that was defined in Eq. (17)

$$\rho = \sum_{k=1}^j \left(\mathcal{F}^{(k)} \tilde{\Phi}^{k-1} \right) \Phi. \quad (24)$$

Eq. (24) is a linear function because $\tilde{\Phi}$ is a known value. Therefore, it is possible to define a pseudo-gradient which

includes the contribution of the high-order terms

$$g_j = \nabla P_C + \sum_{k=2}^j \mathcal{F}^{(k)} \tilde{\Phi}^{k-1}, \quad (25)$$

Now, one can compute the greedy solution of the j^{th} -order constraint

$$[\Phi]_j^b = \frac{\rho}{g_j} \hat{g}_j. \quad (26)$$

With this solution, the new linearization point is selected

$$\tilde{\Phi} = [\Phi]_j^b. \quad (27)$$

Convergence is checked by evaluating the norm of the difference between the solution of iteration b and the previous one, $b-1$

$$\|[\Phi]_j^b - [\Phi]_j^{b-1}\|_2 \leq e_{tol}, \quad (28)$$

where $e_{tol} \in \mathbb{R}$ is an arbitrarily small number. If Eq. (28) is not satisfied, the procedure is repeated from Eq. (24) to Eq. (27). When convergence within the iterations is reached, the truncation order is increased up to the original order of the constraint n .

The flexibility of the method can be exploited to design operation-oriented routines. A nodes-filtering approach is based on the fact that we can rank the entity of the effect a maneuver performed at different times has on PoC using the gradient norm. A dense grid of available thrusting opportunities is built between t_0 and t_{CA} , which is represented by the set $\{t_0, \dots, t_M\}$. First-order maps of PoC are computed with respect to an impulse (or thrust arc) at each point on the grid. If $N \in \mathbb{N}$ is the number of thrust opportunities we want to use, only the first N nodes where the gradient is maximum are kept, while the others are eliminated from the discretization. For example, in Fig. 2, out of the M available maneuvering times, only the second one is kept, and the optimization is run using a single impulse. From this point onward, the algorithm is run as presented in the previous paragraphs using the filtered nodes.

If the maximum thrust is limited, the nodes-filtering routine can be further taken advantage of. The nodes are ranked as explained in the previous paragraph, and, initially, only the first node is kept; if the magnitude of the optimized impulse exceeds the limit imposed by the thrusters, a new reference trajectory is computed subject to a thrust in the optimized direction. A new optimization

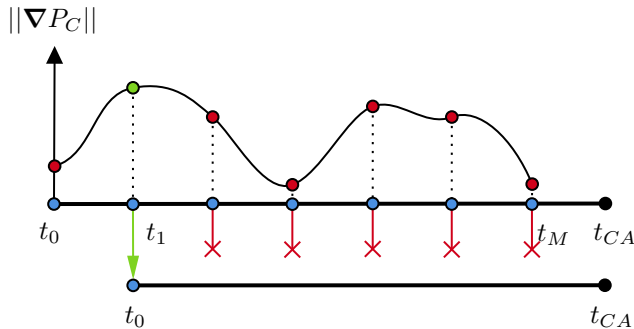


Fig. 2. Maneuvering times ranking and selection routine.

is run with the inclusion of the second-ranked node, considering a reduced PoC gap (ρ) due to the influence of the first insufficient impulse. The process is repeated if necessary until the PoC gap is reduced to 0.

The method can also be used to design optimal maneuvers when the control direction is fixed. This case is common for operators who prefer not to change the attitude of the spacecraft and typically fire in the tangential direction when performing a CAM; in this case, the optimization vector $\Phi \in \mathbb{R}^{N+1}$ includes the magnitude of the impulse (or the continuous thrust) for each thrusting opportunity.

V. RESULTS

The results shown in this section include test cases for low Earth orbit (LEO) and cislunar dynamics. The LEO ones are taken from the ESA Collision Avoidance Challenge, presented in reference [13], which comprises 2170 scenarios. In all the following analyses, $e_{tol} = 10^{-10}$, the target PoC is 10^{-6} , and the dynamics are Keplerian unless otherwise specified. The control components are in radial, along-track, cross-track (RTN) for Earth orbit scenarios and synodic for the Cislunar one. All the simulations are run on an 11th Gen Intel(R) Core(TM) i7-11700

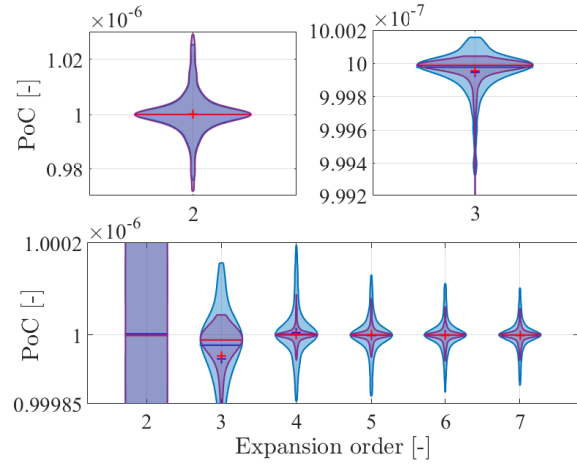


Fig. 3. Distribution of the targeted PoC in the single impulse campaign for the recursive method (blu violins) and fmincon (purple violins).

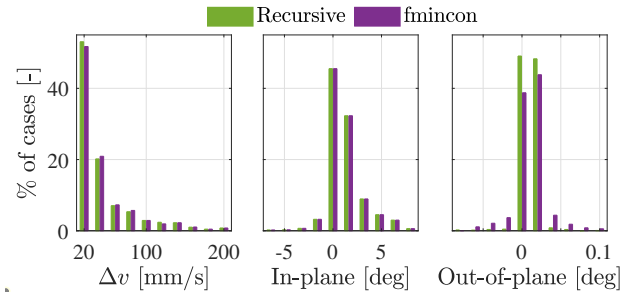


Fig. 4. Distribution of the Δv magnitude and direction for the single-impulse simulation campaign with a 5th-order expansion.

A. Extensive LEO campaign

First, the recursive method is compared in terms of accuracy, i.e., final targeted **PoC**, and computation time, with `fmincon`'s interior-point, used to solve Problem (12). `fmincon` always uses the ballistic trajectory as a first guess. The recovered solution is fed to a forward propagation scheme to validate the results. `fmincon` and the recursive method solve the **NLP** in Problem (12) and the **PP** in Problem (13), respectively, so `fmincon` is expected to provide better results thanks to the fuel-optimal formulation. However, it's worth noticing that the fuel- and energy-optimal formulations coincide in cases of a single impulse or burn. Thus, in the latter case, comparing the two methods provides information about the capability of the recursive method to compute an optimal solution. On the other hand, we can also observe the optimality loss due to the energy-optimal formulation for cases with multiple thrust opportunities. In Fig. 3, the distribution of validated **PoC** after a maneuver performed 2.5 orbits before the encounter is shown for different expansion orders. In the violin plots, the recursive method is represented by the light blue areas and `fmincon` by the purple ones. The mean and median values of the distributions are shown as a cross and a continuous line, respectively: the blue features are relative to the recursive method, the red ones to `fmincon`. The violin plots show

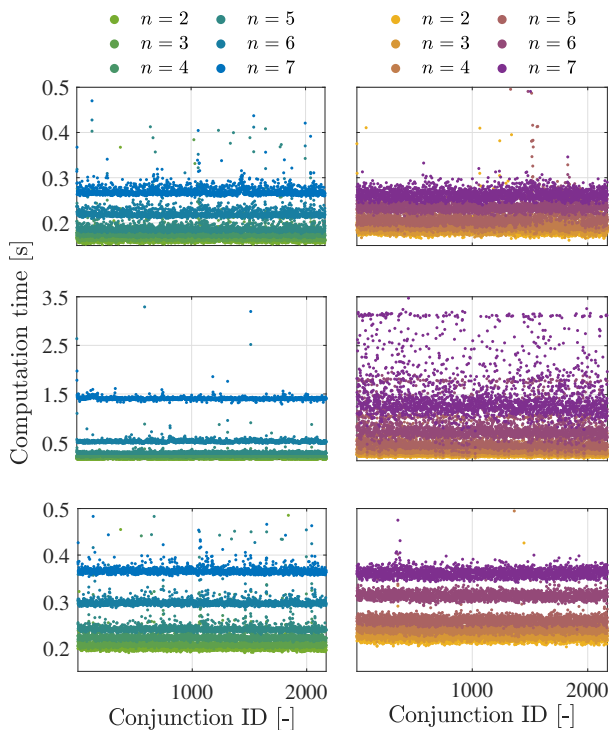


Fig. 5. Computation time for the recursive method (left) and `fmincon` (right). First row: single-impulse campaign. Second row: bi-impulsive campaign. Third-row: J2 campaign.

the 98% of the data. Evidently, the 2nd- and 3rd-order expansions present a larger variance than the following ones, and `fmincon` can target a **PoC** with a higher accuracy. The recursive method becomes very accurate from the 5th-order, showing small improvements for the successive ones. The Δv distribution of the two methods is very similar, as shown in Fig. 4: the preferred direction of most test cases is almost tangential, i.e., with null in-plane and out-of-plane angles, and `fmincon`'s solution typically has a slightly higher out-of-plane component. The computation time, shown in Fig. 5, is typically very similar for the two methods and proportional to the expansion order. The computation of the Taylor expansion Eq. (10) takes up most of the total run time (99% at 2nd-order, 85% at 7th-order). On average, among the 2170 test cases, the number of iterations used by the recursive method with 2nd to 7th-orders are 60, 31, 13, 6, 5, and 5, respectively.

The full dataset of conjunctions is also addressed with a bi-impulsive strategy: the first impulse is at 2.5 orbits before **TCA**, the second one at 0.5. The final **PoC** distribution is very similar to the ones reported in Fig. 3. The second row of Fig. 5 shows that, while for lower expansion orders, the recursive method is only slightly faster, above the 5th order, the computations are significantly faster. In particular, the 5th-order expansion is confirmed as a good choice since its run time is almost always below 0.3 s. Since the number of control variables is doubled, in this case the optimization takes a larger portion of the total run-time: for the 2nd-order the recursive method uses 2% of the run-time, while `fmincon` uses 35%; at the 7th-order the percentages go up to 53% for the recursive and 60% for `fmincon`. In this case, on average, fewer iterations are needed to converge, namely, from 2nd to 7th-orders, 51, 22, 6, 3, 2, and 1. The Δv of the bi-impulsive strategy has a slightly different distribution than the single-impulse counterpart: the recursive method finds slightly higher Δv than `fmincon`, as it solves an energy-optimal problem rather than a fuel-optimal one. As a result, `fmincon` typically finds a solution that is close to a single impulse, while the recursive method always uses both opportunities to fire. If the distributions of the sum of the two Δv are fitted using a Rayleigh curve, the scale parameter of the recursive method is 77.8 mm/s, while `fmincon`'s is 74.2 mm/s.

A last campaign is performed using a more complex dynamics model, with the inclusion of the J2 perturbation. In this case, the final solutions have **PoC** and Δv distributions that are very similar to the ones in Fig. 3 and Fig. 4. As expected, over the course of a few orbits, the inclusion of high-order harmonics does not influence the system's dynamics appreciably. The run-times, shown in the third row of Fig. 5, are generally comparable between the two methods. The increase in the computation time for increasing orders is mainly dictated by the complexity of the **DA** propagation. Once the coefficients are obtained, the two methods perform similarly.

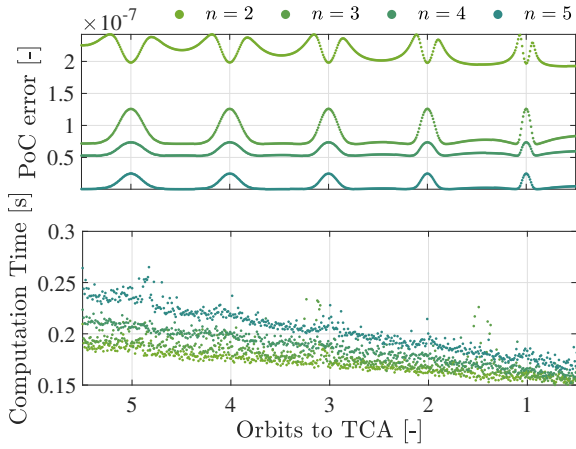


Fig. 6. Targeted PoC and required computation time of the recursive method for different maneuvering times before TCA.

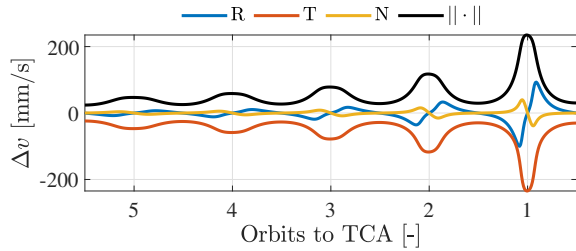


Fig. 7. Evolution of the required Δv for different maneuvering times before TCA using a 5th-order expansion.

B. Single impulse at different times

A detailed analysis of conjunction #1 is performed to determine the optimal firing time between 0.5 and 5.5 orbits before the conjunction. This conjunction represents one of the outliers that were excluded from Fig. 3. Indeed, in the first plot of Fig. 6, one may notice that the targeted PoC error is quite high for low expansion orders. For the 5th-order, PoC is very precise at the half-orbits, but it becomes less accurate at the full orbits. In the full orbits, moreover, the required Δv is much higher than in the half-orbits, as shown in Fig. 7. Fig. 8 shows that a maneuver close to the half-orbit allows the spacecraft to move along the semi-minor axis of the iso-probability ellipse, where the gradient of PoC in the B-plane is higher [14]. At the full orbits, however, the maneuver causes a shift along the ellipse's semi-major axis, where PoC changes less rapidly. For this reason, in agreement with the literature [9, 13, 15, 23], we find that firing at half-orbits is best for fuel efficiency. From the second plot in Fig. 6, it is confirmed that the 5th-order expansion offers the optimal balance between accuracy and computation speed.

C. Low-thrust maneuver

The analysis performed on the whole set of conjunctions using the low-thrust model with a single firing opportunity is similar to the impulsive case and is not reported for brevity. Instead, we report an analysis encom-

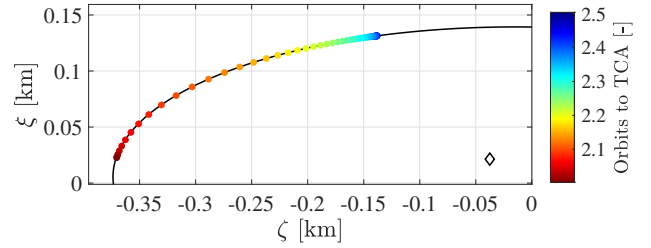


Fig. 8. B-plane configuration in conjunction #1 for different maneuvering times using a 5th-order expansion. The diamond is the ballistic relative position at TCA, and the scattered points indicate the position after the maneuver.

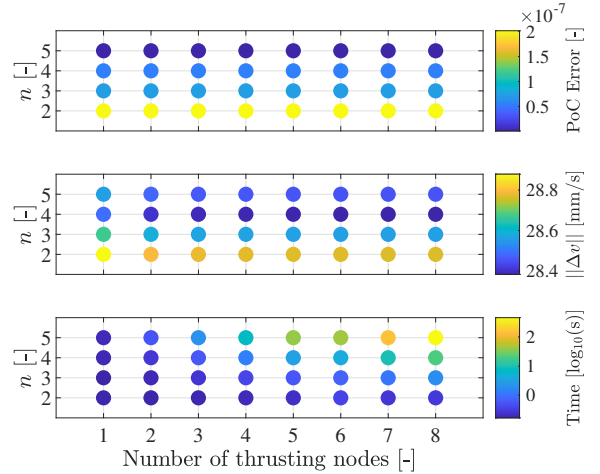


Fig. 9. Accuracy, required Δv , and computation time for a single low-thrust window with different discretization points and expansion orders.

passing a different discretization of the thrusting window using different expansion orders. The considered test case is still conjunction #1. The thrusting window is centered around 2.5 orbits before TCA, spans 6 minutes, and is discretized in a number of nodes that varies from 1 to 8. The denser the discretization grid is, the more accurate the maneuver can be in terms of thrusting direction. The first plot in Fig. 9 shows that the accuracy of the maneuver is independent of the number of discretization nodes. Moreover, the sensitivity of the total required Δv to the number of nodes is very low, too. Given that the computation time, shown in the last plot, grows proportionally to the two variables, a low number of discretization nodes is preferable in this case.

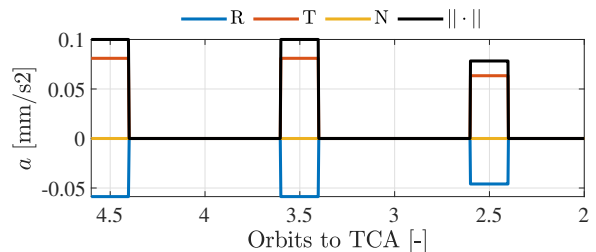


Fig. 10. Acceleration profile using the nodes-filtering routine in conjunction #1219.

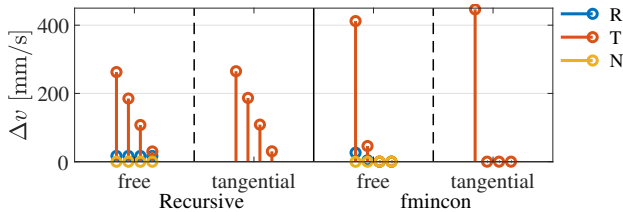


Fig. 11. Tetra-impulsive optimization comparison between the recursive method and fmincon with and without fixed tangential direction.

Let us now consider conjunction #1219, for which the required Δv from the campaign in Section A is high (342.5 mm/s). The maximum acceleration of a 500 kg satellite mounting a 50 mN thruster is 0.1 mm/s^2 . This means that to achieve 342.5 mm/s one should thrust for almost 1 hour, which is more than half the orbital period. So, the maneuver must be split into multiple thrust arcs over multiple orbits. Given a series of available thrust arcs, centered at every half-orbit from 5 orbits before TCA and lasting for 20 minutes, we can apply the nodes-filtering routine to optimize the maneuver. The resulting thrust profile, shown in Fig. 10, grants a targeting of PoC with an absolute precision of 10^{-10} : only the first three thrust windows are used. This is not a bang-bang profile, but it can be easily regularized by slightly reducing the thrust time in the last window.

D. Fixed direction

Space operators might prefer to thrust in a fixed direction to simplify attitude control. Knowing that when sufficient warning time is given, the tangential direction is the most efficient for CAM, working with a fixed tangential thrust might simplify the maneuver implementation with little sacrifice in optimality. Additionally, fixing the direction reduces the problem variables to 1/3 of an unconstrained problem, thus improving numerical efficiency. To exemplify this, let us consider conjunction #1,466 from the dataset, which is one of the most demanding. Keeping the 5th-order expansion, we compare performances of fmincon and the recursive method using free-direction optimization (optimizing the three thrust components) or tangential impulses. Namely, impulses are available 3.5, 2.5, 1.5 and 0.5 orbital periods before TCA. As can be seen from Fig. 11, when multiple impulses are available, the recursive method finds a solution that uses every available opportunity to fire because the gradient of PoC is non-null with respect to each thrusting window. On the contrary, fmincon, solving the fuel-optimal problem, uses as few impulses as possible: in the tangential firing case, only one impulse is used. In every case, the validated final PoC value is achieved with an absolute precision of 10^{-10} . While obtaining the same accuracy and finding a similar solution, the fixed-direction optimization is much faster than the free-direction one, keeping the execution time below 0.4 s both using fmincon (0.38 s vs 3.41 s) and the recursive method (0.26 s vs 0.86 s). This significant

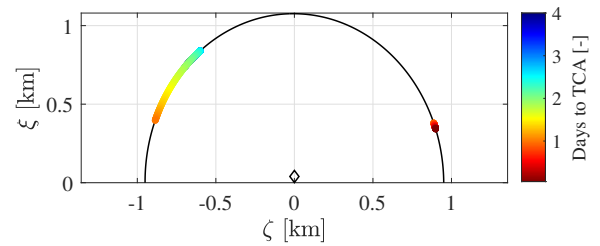


Fig. 12. B-plane configuration in the cislunar test-case for different maneuvering times using a 2nd-order expansion. The blue kernels are hidden behind the light blue ones.

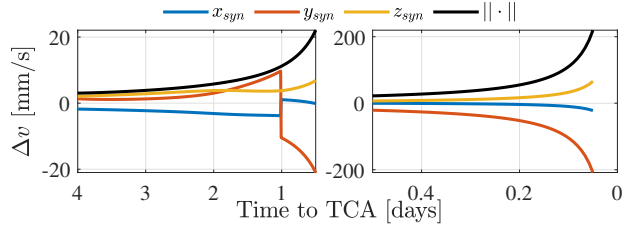


Fig. 13. Evolution of the required Δv for different maneuvering times before TCA using a 2nd-order expansion in the cislunar test case.

increase in efficiency comes at a very low loss in terms of optimality: the total Δv is only increased by 1.2 mm/s using the recursive method and 12.6 mm/s with fmincon.

E. Cislunar dynamics

The single-impulse optimization is applied to a L1-Near Rectilinear Halo Orbit from reference [24] to showcase the applicability to the cislunar domain. The 2nd-order expansion is accurate enough in this application, reaching very similar values of final PoC compared to higher orders. In Fig. 12, the positions reached on the B-plane for maneuvering times spanning from 4 days to 1 hour before TCA are shown. In Fig. 13, the required impulsive Δv components are presented. The results are very similar to the ones obtained with the analytical methods from [24]. In particular, both algorithms find two different optimal wells that are targeted alternatively depending on the alert time: in the first three days, the region in the second quadrant of the B-plane is targeted, while for shorter alert times, the region in the first quadrant is preferred. The computational time is comparable to the LEO test cases: out of the 500 simulations performed to analyze the test case, the mean execution time was 0.153 s, with a standard deviation of 0.005 s.

VI. CONCLUSIONS

A recursive method for the design of a collision avoidance maneuver (CAM) was presented based on the polynomial expansion of the probability of collision (PoC). The method is generally applicable to scenarios involving a single short-term encounter with any dynamics, and it can deal with an arbitrary number of different maneuvering windows. Moreover, it can deal both with low-thrust and with impulsive dynamics, optimizing the

control acceleration of the thrust arc in the first case and the impulses in the second.

The computational results showcase various combinations of CAM dynamics, thrust models, maneuvering times, and expansion orders. The recursive method's solution to the energy-optimal polynomial program is compared with fmincon's, which is a solution to the fuel optimal nonlinear program. Very similar results are obtained by the two methods in most of the cases: a target PoC is almost always achieved with very high accuracy, and the computational time is usually kept below 1 s. The simplicity and immediateness of the method, combined with the quasi-optimal results that it can achieve, make it potentially suitable for onboard implementation.

REFERENCES

- [1] ESOC. ESA's Annual Space Environment Report. Technical report, ESA, 2023.
- [2] Russell P. Patera and Glenn E. Peterson. Space vehicle maneuver method to lower collision risk to an acceptable level. *Journal of Guidance, Control, and Dynamics*, 26(2):233–237, 2003.
- [3] Salvatore Alfano and Lake Tahoe. Collision Avoidance Maneuver Planning Tools. In *15th AAS/AIAA Astrodynamics Specialist Conference*. Lake Tahoe, California, 2005.
- [4] Saika Aida. Conjunction Risk Assessment and Avoidance Maneuver Planning Tools. feb 2016.
- [5] Ignacio Grande-Olalla, Noelia Sanchez-Ortiz, Juan Antonio Pulido, and Klaus Merz. Collision risk assesment and avoidance manoeuvres. New tool coram for esa. Technical report, 2013.
- [6] Alessandro Morselli, Roberto Armellin, Pierluigi Di Lizia, Franco Bernelli Zazzera, and F. Bernelli-Zazzera. Collision avoidance maneuver design based on multi-objective optimization. In *AIAA/AAS Astrodynamics Specialist Conference 2014*, volume 152, pages 1819–1838. San Diego, California, 2014.
- [7] Claudio Bombardelli. Analytical formulation of impulsive collision avoidance dynamics. *Celestial Mechanics and Dynamical Astronomy*, 118(2):99–114, 2014.
- [8] Javier Hernando-Ayuso and Claudio Bombardelli. Low-thrust collision avoidance in circular orbits. *Journal of Guidance, Control, and Dynamics*, 44(5):983–995, may 2021.
- [9] Claudio Bombardelli and Javier Hernando-Ayuso. Optimal impulsive collision avoidance in low earth orbit. In *Journal of Guidance, Control, and Dynamics*, volume 38, pages 217–225, feb 2015.
- [10] Andrea De Vittori, Maria Francesca Palermo, Pierluigi Di Lizia, and Roberto Armellin. Low-Thrust Collision Avoidance Maneuver Optimization. *Journal of Guidance, Control, and Dynamics*, 45(10):1815–1829, oct 2022.
- [11] Stéphane Mazouffre. Electric propulsion for satellites and spacecraft: Established technologies and novel approaches. *Plasma Sources Science and Technology*, 25(3), 2016.
- [12] Shrouti Dutta and Arun K. Misra. Convex optimization of collision avoidance maneuvers in the presence of uncertainty. *Acta Astronautica*, 197:257–268, aug 2022.
- [13] Roberto Armellin. Collision avoidance maneuver optimization with a multiple-impulse convex formulation. *Acta Astronautica*, 186:347–362, sep 2021.
- [14] Zeno Pavanello, Laura Pirovano, and Roberto Armellin. Long-Term Encounters Collision Avoidance Maneuver Optimization with a Convex Formulation. In *33rd AAS/AIAA Space Flight Mechanics Meeting*, pages 1–20. Austin, TX, 2023.
- [15] Zeno Pavanello, Laura Pirovano, Roberto Armellin, Andrea De Vittori, and Pierluigi Di Lizia. A Convex Optimization Method for Multiple Encounters Collision Avoidance Maneuvers. In *AIAA SciTech Forum*, number January, pages 1–17. Orlando, Florida, 2024.
- [16] Zeno Pavanello, Laura Pirovano, Roberto Armellin, Andrea De Vittori, and Pierluigi Di Lizia. A Convex Formulation for Collision Avoidance Maneuver Strategies During Low-Thrust Phases. In *AIAA SciTech Forum*, number January, pages 1–19. Orlando, Florida, 2024.
- [17] Ryan S. Park and Daniel J. Scheeres. Nonlinear Mapping of Gaussian Statistics: Theory and Applications to Spacecraft Trajectory Design. *Journal of Guidance, Control, and Dynamics*, 29(6):1367–1375, nov 2006.
- [18] Jia Sheng Li, Zhen Yang, and Ya Zhong Luo. A review of space-object collision probability computation methods. *Astrodynamics*, 6(2):95–120, jun 2022.
- [19] Ken Chan. International Space Station Collision Probability. *The Aerospace Corporation, Chantilly, VA, USA*, 6(2):307–314, 2009.
- [20] Jagadish Singh and Joel John Taura. Motion in the generalized restricted three-body problem. *Astrophysics and Space Science*, 343(1):95–106, 2013.
- [21] R. Armellin, P. Di Lizia, F. Bernelli-Zazzera, and M. Berz. Asteroid close encounters characterization using differential algebra: The case of Apophis. *Celestial Mechanics and Dynamical Astronomy*, 107(4):451–470, 2010.
- [22] Erica L. Jenson and Daniel J. Scheeres. Bounding nonlinear stretching about spacecraft trajectories using tensor eigenpairs. *Acta Astronautica*, 214(October 2023):159–166, 2024.
- [23] Andrea De Vittori, Gabriele Dani, Pierluigi Di Lizia, and Roberto Armellin. Numerically Efficient Methods for Low Thrust Collision Avoidance Maneuver Design in LEO Regime. In *AAS/AIAA Space Flight Mechanics Meeting*. 2023.
- [24] Luigi De Maria, Andrea De Vittori, and Pierluigi Di Lizia. Numerically Efficient Impulsive and Low-Thrust Collision Avoidance Manoeuvres in Cislunar L1-Near Rectilinear Halo Orbit. In *74th International Astronautical Congress (IAC)*. Baku, Azerbaijan, 2023.



Zeno Pavanello obtained his B.Sc. degree in Aerospace Engineering from the University of Padua in 2017. He obtained his M.Sc. double degree in Aerospace Engineering in 2020 from the University of Padua and the Instituto Superior Técnico of Lisbon. Zeno is currently a third-year Ph.D. student at Te Pūnaha Ōtea – Space Institute at the University of Auckland. He works on collision avoidance maneuvers optimization.



Laura Pirovano received her M.Sc. degree in aerospace engineering (space exploration track) from TU Delft, the Netherlands, in 2015. She completed her Ph.D. at the University of Surrey, UK, in 2020 on methods for cataloging space debris with optical observations. She is now a research fellow at Te Pūnaha Ōtea – Space Institute at the University of Auckland. Her research interests include space situational awareness and uncertainty propagation.



Roberto Armellin received his M.Sc. and Ph.D. degrees in aerospace engineering from Politecnico di Milano, Italy, in 2003 and 2007, respectively. Since November 2020, he has been a professor at Te Pūnaha Ōtea – Space Institute, the University of Auckland. His current research interests include space trajectory optimization, spacecraft navigation and guidance, and space situational awareness.